# FROM DESIGN TO CONTROL: DEVELOPMENT AND EXPERIMENTAL VALIDATION OF A MEDICAL ROBOTICS ARM

*Zou Han*

Department of Surgical & Interventional Engineering
School of Biomedical Engineering & Imaging Sciences
Faculty of Life Sciences & Medicine
King's College London, London, UK
K24012533@kcl.ac.uk

**Abstract.** This study aims to develop a two-degree-of-freedom (2-DOF) medical robotic arm system through CAD modeling and 3D printing for structural design, integrating Arduino microcontrollers, DC motors, sensors, and H-Bridge motor driver modules for hardware implementation. The system employs a PID control algorithm for parameter tuning, combined with forward/inverse kinematics and the Jacobian matrix for trajectory planning. Experimental validation includes target point tracking and multi-point path tracking, utilizing real-time MATLAB-Arduino communication for control and data visualization. The results demonstrate that the system exhibits high stability and precise path-tracking capabilities under PID control, effectively reducing tracking errors while showing strong responsiveness across varying control parameters. Future work will explore adaptive control algorithms to optimize PID parameters, further enhancing real-time responsiveness and tracking accuracy in complex scenarios. Overall, this study successfully achieves an end-to-end workflow from design to control, validating the system's feasibility and effectiveness in medical task scenarios, laying a technical foundation for future optimization and practical clinical applications.

## 1. INTRODUCTION

With the rapid advancement of medical robotics technology, robotic systems have become essential tools in modern healthcare. As highlighted in studies [1,2], these systems offer unprecedented precision, stability, and reliability in minimally invasive surgery and medical diagnostics. In this context, two-degree-of-freedom (2-DOF) robotic systems have emerged as key enablers in tasks requiring fine control and high-precision positioning, such as needle insertion [3] , tissue manipulation, and surgical tool alignment [4].

However, 2-DOF medical robotic arms still face several challenges in their design and application. Firstly, the structural design must achieve an optimal balance between flexibility, lightweight properties, and structural stability [5] to ensure stable operational performance in complex surgical environments. Secondly, the feedback control system requires further optimization in terms of real-time response and control precision [6], addressing the stringent requirements of high-precision minimally invasive surgery. Furthermore, although PID (Proportional-Integral-Derivative) control algorithms have demonstrated excellent performance in path tracking and error compensation, there is still room for improvement in adaptive parameter tuning and dynamic response optimization [7].

While alternative control algorithms, such as Model Predictive Control (MPC) and Sliding Mode Control (SMC), have been proposed to address these limitations, they often suffer from computational complexity [8] and Chattering Phenomenon [9]. These limitations restrict their broader application in time-sensitive surgical tasks, where immediate feedback and rapid adjustment are critical.

To address these challenges, this study aims to enhance the structural design of the robotic arm, optimize the feedback control system, and improve the PID control algorithm. The structural design is achieved through CAD modeling and 3D printing, while hardware implementation integrates Arduino microcontrollers, DC motors, sensors, and H-Bridge motor driver modules. The control system employs a PID control algorithm for parameter tuning, combined with forward/inverse kinematics and the Jacobian matrix for trajectory planning. Real-time communication between MATLAB and Arduino is utilized to enable control and data visualization. Experimental validation includes target point tracking and multi-point path tracking, demonstrating that the system, under PID control, exhibits high stability and precise path-tracking capabilities, effectively reducing tracking errors and showing strong responsiveness under varying control parameters.

Future work will further explore adaptive control algorithms, leveraging existing research [10] to optimize PID parameters, thereby enhancing the system's real-time responsiveness and tracking accuracy in complex scenarios. Overall, this study successfully achieves an end-to-end workflow from structural design to control implementation, validating the system's feasibility and effectiveness in medical task scenarios and laying a solid technical foundation for future optimization and practical clinical applications.

## 2. Methodology

### 2.1 System Design

The CAD design of the two-degree-of-freedom (2-DOF) medical robotic arm system is carefully structured to balance space utilization, structural stability, and ease of maintenance.

The hardware components, including the Arduino microcontroller, DC motors, sensors, and H-Bridge motor driver modules, are carefully selected and integrated to support the system's structural and functional design (refer to the hardware list in Table 1).

| Hardware | Specification/Details | Function |
|---|---|---|
| Arduino UNO *1 | Microcontroller with 14 digital I/O pins, 6 analog inputs, operating voltage: 5V | Central control unit for managing motor control and sensor data processing |
| DC Motors *2 | Operating voltage: 6-12V, Speed: 90 RPM, Torque: 70 oz-in Weight: 12g | Provides actuation for the two degrees of freedom |
| L298N Dual H-Bridge Motor Driver Module *1 | Max input voltage: 46V Peak output current (each Channel): 3A DC max output current (each Channel): 2A | Controls motor direction and speed |
| INA169 current sensor | Input Voltage Range: 2.7V to 60V | Protecting motors, improving control precision, and optimizing energy efficiency |
| others | Screws, F-M cables, USB cable | Combination supports |

TABLE 1 Hardware List

#### 2.1.1 Base Design and Hardware Integration

The base (see Figure 1), with dimensions of 110mm × 80mm × 90mm, incorporates a modular slot design for efficient assembly and debugging. It features a dual-layer layout: the first layer houses the Arduino UNO, while the second layer accommodates the dual H-Bridge motor driver module, optimizing space and ensuring component organization. A 5V power supply is directly soldered onto a compact chip to save space and enhance power stability, eliminating the need for a breadboard. The Arduino serves as the primary control unit, processing sensor data and controlling motor direction and speed through the H-Bridge motor driver. All components are connected via soldering and modular interfaces, ensuring reliable signal transmission and compact integration, forming a robust foundation for system stability.

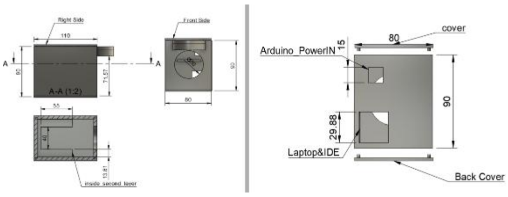


Figure 1: Base Design of Robotic Arm Components (all dimensions in mm)

### 2.1.2 Arm Design

The robotic arm consists of Arm1 and Arm2, achieving a balance between stability and lightweight design. Arm1 demonstrates structural stability (see Figure 2(a)), while Arm2 features a lightweight structure with precise axis alignment (see Figure 2(b)). During the design process, careful consideration was given to the outer diameter and overlapping length of the joints, resulting in effective lengths of approximately 96mm for Arm1 and 60mm for Arm2, enabling the robotic arm to reach a maximum working range of 156mm, meeting the requirements of most precision control tasks [11].

Arm1 adopts a thicker structure to provide enhanced load-bearing capacity, while Arm2 utilizes a flat, lightweight design to reduce endpoint load pressure and minimize the risk of structural deformation. This dual-arm design ensures precision and flexibility in practical applications, providing a reliable foundation for medical tasks.

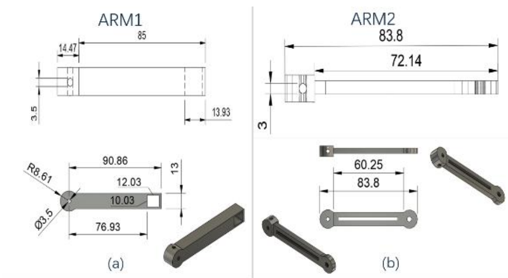


Figure 2: CAD Design of Robotic Arm Components (all dimensions in mm)

### 2.1.3 Penholder Design

The penholder follows a lightweight design principle (see Figure 3), which reduces stress on Arm2, further minimizing the risk of structural deformation. The axis alignment of the penholder coincides with Arm2's rotational axis, effectively reducing positional offset errors during testing and improving precision.

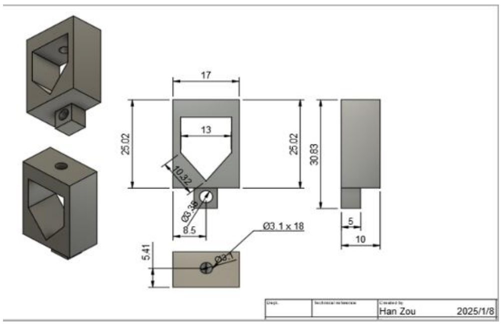


Figure 3: Penholder Design of Robotic Arm Components (all dimensions in mm)

### 2.1.4 3D Printing Parameters

The detailed printing specifications, including layer height, print angle, and structural support strategies, are comprehensively presented in *Table 2* for clarity and reference.

| Component | Parameters | Design Features |
|---|---|---|
| Base | 0.28mm layer height, 0.2mm first-layer height, 2 wall layers | Tree supports to ensure accurate printing of hollow structures |
| Arms and Penholder | 45° printing angle | Enhanced surface smoothness and structural strength |
| Connector | Slot-based design, compatible with RC motor drive shaft | 3.5mm screw fixation, considering 3D printing tolerance errors |

TABLE 2 3D Printing Parameters and Connector Design (all dimensions in mm)

### 2.1.5 Connector Design

All joints and connectors utilize a slot-based design that perfectly fits the RC motor's drive shaft. A 3.5mm screw securely fastens one side of the D-shaft, while the motor body is housed in a square slot measuring 12.03mm × 10.03mm. This precise slot dimension accounts for 3D printing tolerances, ensuring a snug fit for the DC motor. The end-effector (penholder) is secured using 3.5mm screws and nuts, enhancing overall reliability and facilitating easy maintenance and scalability for potential mass production.

Overall, this CAD design achieves a balance between functionality, stability, and manufacturability, providing a robust foundation for the robotic arm's hardware integration and control systems.

## 2.2 Low-Level Motor Control

### 2.2.1 PID Control Algorithm

The PID control algorithm combines three components—Proportional (P), Integral (I), and Derivative (D)—to regulate the dynamic response of the robotic arm.

The PID controller can be mathematically described using the following transfer function:

$$G_c(s) = K_p + \frac{K_i}{s} + K_d s$$

To regulate the system's behavior, the error e(t), defined as the difference between the reference r(t) and the output y(t), is minimized:

$$e(t) = r(t) - y(t)$$

The output, u$(t)$, is mathematically represented as:

$$u(t)=K_p e(t) + K_i \int e(t)dt + K_d \frac{de(t)}{dt}$$

where:

i. e(t): Error signal (difference between the target and actual position).
ii. $K_p$ ,$K_i$ ,$K_d$ : Gains for proportional, integral, and derivative components.

This formulation ensures that the robotic arm can dynamically adjust its response to achieve the desired joint angles with high precision.

### 2.2.2 Parameter Tuning and The Results

Parameter tuning is a crucial step in ensuring the performance of the PID control algorithm. By iteratively adjusting the gain parameters ($K_p$, $K_i$, $K_d$), observing the system's dynamic response, and recording the resulting data (see Table 3), the optimal parameters were determined, and the response curve was plotted (see Figure 4 and Figure 5). After comparison, the most accurate final value with relatively small oscillation was selected.

*Note:

P – spring: to move to the reference faster.

D – damping (friction): to reduce speed and oscillations

I – integral: to accumulate error to reduce steady-state error

Max_V: represents the peak value of the system's response during overshoot, occurring at the peak time (Tp)

Min_V: represents the lowest value of the system's response during undershoot, occurring at the minimum time (Tm)

Error_V: Represents the difference between the desired angle and the system's actual response value.

Final_V: Represents the system's actual response value.

Max_V and Min_V are crucial for evaluating overshoot behavior and stability, guiding PID parameter adjustments to minimize overshoot and improve control precision.

| | P | D | I | Max_V | Min_V | Error_V | Final_V |
|---|---|---|---|---|---|---|---|
| motor1 | 20.00 | 0.00 | 0.00 | 124.57 | 73.07 | -7.44 | 97.44 |
| | 19.00 | 0.00 | 0.00 | 126.97 | 77.86 | 10.95 | 79.05 |
| | 19.00 | 0.10 | 0.00 | 123.37 | 82.65 | 6.15 | 83.85 |
| | 19.00 | 0.20 | 0.00 | 123.37 | 80.25 | 8.55 | 81.45 |
| | 20.00 | 0.20 | 0.00 | 129.36 | 68.27 | 0.17 | 89.83 |
| | 20.00 | 0.25 | 0.00 | 129.36 | 73.07 | 2.56 | 87.44 |
| | 19.00 | 0.25 | 0.00 | 124.57 | 76.66 | 4.96 | 85.04 |
| | 19.00 | 0.20 | 0.00 | 126.97 | 71.87 | 3.76 | 86.24 |
| | 19.00 | 0.20 | 0.00 | 124.57 | 73.07 | 4.96 | 85.04 |
| | 18.00 | 0.15 | 0.00 | 126.97 | 74.26 | 6.15 | 83.85 |
| | 18.00 | 0.10 | 0.00 | 125.77 | 76.66 | 9.75 | 80.25 |
| | 18.00 | 0.17 | 0.00 | 125.77 | 76.66 | 7.35 | 82.65 |
| | 18.00 | 0.18 | 0.00 | 128.16 | 74.26 | 4.96 | 85.04 |
| | 21.00 | 0.30 | 0.00 | 129.47 | 68.28 | 2.95 | 87.05 |
| | 19.00 | 0.60 | 0.00 | 125.77 | 74.26 | 3.76 | 86.24 |
| | 20.00 | 0.20 | 0.00 | 128.16 | 71.87 | 2.56 | 87.44 |
| | 16.00 | 0.18 | 0.00 | 128.16 | 64.68 | 0.17 | 89.83 |
| motor2 | 20.00 | 0.00 | 0.00 | -100.90 | -83.78 | 0.83 | -90.83 |
| | 18.00 | 1.00 | 0.00 | -100.79 | -84.79 | 1.23 | -91.23 |
| | 17.00 | 1.00 | 0.00 | -100.29 | -85.17 | 0.83 | -90.83 |
| | 17.00 | 0.50 | 0.00 | -100.70 | -85.39 | 0.22 | -90.22 |
| | 17.00 | 0.40 | 0.00 | -100.70 | -84.99 | 0.83 | -90.83 |
| | 16.00 | 0.50 | 0.00 | -100.90 | -85.19 | 0.63 | -90.63 |
| | 17.00 | 0.75 | 0.00 | -101.30 | -84.99 | 0.83 | -90.83 |
| | 17.00 | 0.60 | 0.00 | -100.70 | -85.59 | 0.02 | -90.02 |
| | 16.80 | 0.60 | 0.00 | -100.50 | -85.79 | -0.38 | -89.62 |
| | 16.80 | 0.58 | 0.00 | -100.29 | -85.79 | -0.38 | -89.62 |

TABLE 2 Gain Parameter Tuning Results for PID Controller

Motor1

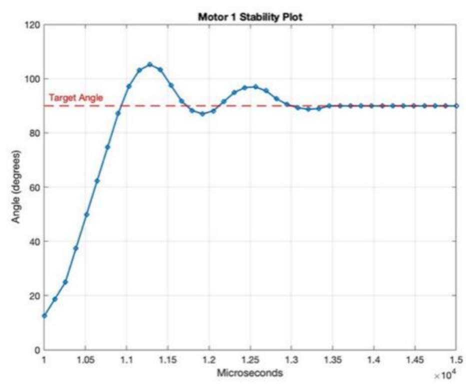

Figure 4: Time Response of Motor1

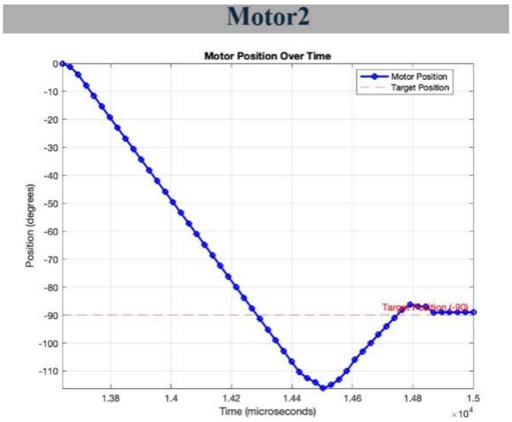


Figure 5: Time Response of Motor2

results

The optimization process successfully balanced precision and stability, as reflected in the response curves (Figures 2.4 and 2.5). The final parameters, summarized in Table 2.3, demonstrated:

- Rapid convergence to the target position.
- Minimal oscillatory behavior.
- Reduced steady-state error.

This tuning methodology ensured the PID controller achieved precise and stable control of the robotic arm, meeting the requirements for complex applications. Key metrics such as Max_V, Min_V, Error_V, and Final_V were instrumental in evaluating performance and guiding parameter adjustments to achieve optimal results.

| | P | D | I | Max_V | Min_V | Error_V | Final_V |
|---|---|---|---|---|---|---|---|
| motor1 | 20.00 | 0.00 | 0.00 | 124.57 | 73.07 | -7.44 | 97.44 |
| | 19.00 | 0.00 | 0.00 | 126.97 | 77.86 | 10.95 | 79.05 |
| | 19.00 | 0.10 | 0.00 | 123.37 | 82.65 | 6.15 | 83.85 |
| | 19.00 | 0.20 | 0.00 | 123.37 | 80.25 | 8.55 | 81.45 |
| | 20.00 | 0.20 | 0.00 | 129.36 | 68.27 | 0.17 | 89.83 |
| | 20.00 | 0.25 | 0.00 | 129.36 | 73.07 | 2.56 | 87.44 |
| | 19.00 | 0.25 | 0.00 | 124.57 | 76.66 | 4.96 | 85.04 |
| | 19.00 | 0.20 | 0.00 | 126.97 | 71.87 | 3.76 | 86.24 |
| | 19.00 | 0.20 | 0.00 | 124.57 | 73.07 | 4.96 | 85.04 |
| | 18.00 | 0.15 | 0.00 | 126.97 | 74.26 | 6.15 | 83.85 |
| | 18.00 | 0.10 | 0.00 | 125.77 | 76.66 | 9.75 | 80.25 |
| | 18.00 | 0.17 | 0.00 | 125.77 | 76.66 | 7.35 | 82.65 |
| | 18.00 | 0.18 | 0.00 | 128.16 | 74.26 | 4.96 | 85.04 |
| | 21.00 | 0.30 | 0.00 | 129.47 | 68.28 | 2.95 | 87.05 |
| | 19.00 | 0.60 | 0.00 | 125.77 | 74.26 | 3.76 | 86.24 |
| | 20.00 | 0.20 | 0.00 | 128.16 | 71.87 | 2.56 | 87.44 |
| | 16.00 | 0.18 | 0.00 | 128.16 | 64.68 | 0.17 | 89.83 |
| motor2 | 20.00 | 0.00 | 0.00 | -100.90 | -83.78 | 0.83 | -90.83 |
| | 18.00 | 1.00 | 0.00 | -100.79 | -84.79 | 1.23 | -91.23 |
| | 17.00 | 1.00 | 0.00 | -100.29 | -85.17 | 0.83 | -90.83 |
| | 17.00 | 0.50 | 0.00 | -100.70 | -85.39 | 0.22 | -90.22 |
| | 17.00 | 0.40 | 0.00 | -100.70 | -84.99 | 0.83 | -90.83 |
| | 16.00 | 0.50 | 0.00 | -100.90 | -85.19 | 0.63 | -90.63 |
| | 17.00 | 0.75 | 0.00 | -101.30 | -84.99 | 0.83 | -90.83 |
| | 17.00 | 0.60 | 0.00 | -100.70 | -85.59 | 0.02 | -90.02 |
| | 16.80 | 0.60 | 0.00 | -100.50 | -85.79 | -0.38 | -89.62 |
| | 16.80 | 0.58 | 0.00 | -100.29 | -85.79 | -0.38 | -89.62 |

**TABLE 2.3:** Gain Parameter Tuning Results for PID Controller

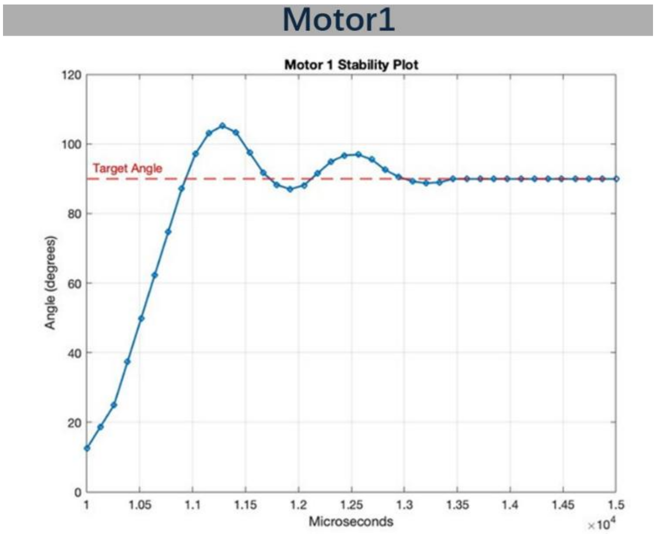


**Figure 2.4:** Time Response of Motor1

# Motor2

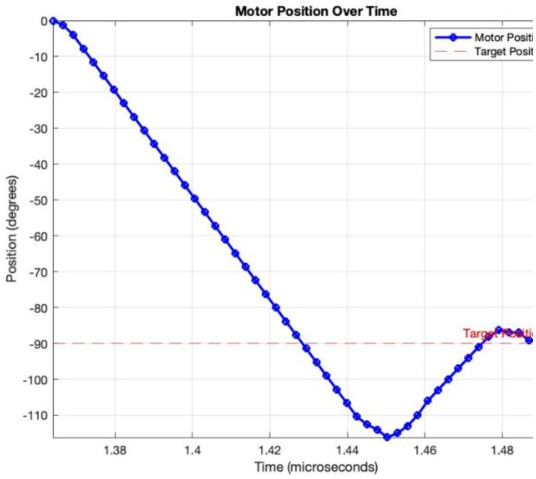

Motor Position Over Time
Motor Positi
Target Posit
Position (degrees)
0
-10
-20
-30
-40
-50
-60
-70
-80
-90
-100
-110
1.38
1.4
1.42
1.44
1.46
1.48
Time (microseconds)

## Reference


[1] C. Walther, S. Fichtlscherer, T. Holubec, M. Vasa-Nicotera, M. Arsalan, and T. Walther, 'New developments in transcatheter therapy of mitral valve disease', *J Thorac Dis*, vol. 12, no. 4, pp. 1728–1739, Apr. 2020, doi: 10.21037/jtd.2019.12.137.

[2] P. Picozzi *et al.*, 'Advances in Robotic Surgery: A Review of New Surgical Platforms', *Electronics*, vol. 13, no. 23, p. 4675, Nov. 2024, doi: 10.3390/electronics13234675.

[3] C. Yang, Y. Xie, S. Liu, and D. Sun, 'Force Modeling, Identification, and Feedback Control of Robot-Assisted Needle Insertion: A Survey of the Literature', *Sensors*, vol. 18, no. 2, p. 561, Feb. 2018, doi: 10.3390/s18020561.

[4] M. G. Fujie and B. Zhang, 'State-of-the-art of intelligent minimally invasive surgical robots', *Front. Med.*, vol. 14, no. 4, pp. 404–416, Aug. 2020, doi: 10.1007/s11684-020-0743-3.

[5] H. M. Tuan, F. Sanfilippo, and N. V. Hao, 'Modelling and Control of a 2-DOF Robot Arm with Elastic Joints for Safe Human-Robot Interaction', *Front. Robot. AI*, vol. 8, p. 679304, Aug. 2021, doi: 10.3389/frobt.2021.679304.

[6] P. Kormushev, Y. Demiris, and D. G. Caldwell, 'Kinematic-free position control of a 2-DOF planar robot arm', in *2015 IEEE/RSJ International Conference on Intelligent Robots and Systems (IROS)*, Hamburg, Germany: IEEE, Sep. 2015, pp. 5518–5525. doi: 10.1109/IROS.2015.7354159.

[7] O. M. Omisore, T. Akinyemi, W. Duan, W. Du, and L. Wang, 'A Novel Sample-efficient Deep Reinforcement Learning with Episodic Policy Transfer for PID-Based Control in Cardiac Catheterization Robots', Oct. 28, 2021, *arXiv*: arXiv:2110.14941. doi: 10.48550/arXiv.2110.14941.

[8] S. Richter, C. N. Jones, and M. Morari, 'Computational Complexity Certification for Real-Time MPC With Input Constraints Based on the Fast Gradient Method', *IEEE Trans. Automat. Contr.*, vol. 57, no. 6, pp. 1391–1403, Jun. 2012, doi: 10.1109/TAC.2011.2176389.

[9] C. Jing, H. Zhang, Y. Liu, and J. Zhang, 'Adaptive Super-Twisting Sliding Mode Control for Robot Manipulators with Input Saturation', *Sensors*, vol. 24, no. 9, p. 2783, Apr. 2024, doi: 10.3390/s24092783.

[10] X. Zhang and Y. Yang, 'Optimization of PID controller parameters using a hybrid PSO algorithm', *Int. J. Dynam. Control*, vol. 12, no. 10, pp. 3617–3627, Oct. 2024, doi: 10.1007/s40435-024-01455-y.

[11] I. Meir, A. Bechar, and A. Sintov, 'Kinematic Optimization of a Robotic Arm for Automation Tasks with Human Demonstration', in *2024 IEEE International Conference on Robotics and Automation (ICRA)*, Yokohama, Japan: IEEE, May 2024, pp. 7172–7178. doi: 10.1109/ICRA57147.2024.10610924.